*International Research Journal of Environmental Sciences*_____ ISSN 2319–1414
Vol. **15(4),** 75-84, October **(2026)** *Int. Res. J. Environmental Sci.*

Mathematical Modeling, Energy and Exergy Analysis of a Solar Air Collector under Variable Operating and Climatic Conditions

Ibragimov Umidjon Khikmatullayevich*, Avanesov Tigran Rubenovich and Mirzayorova Sevara Ubaydullayevna
Karshi state technical university, Karshi, Uzbekistan
ibragimov_u@rambler.ru

Available online at: www.isca.in, www.isca.me
Received 28th August 2026, revised 29th September 2026, accepted 13th October 2026

Abstract

This research presents a mathematical model for assessing the energy and exergy performance of a turbulator-equipped solar air heater (SAH) subjected to changing climatic and operating conditions. The model incorporates variations in solar irradiance, ambient temperature, and air mass flow rate, together with thermal losses, heat exchange between the absorber and air, and airflow resistance. Simulations were conducted for Qarshi from 08:00 to 18:00 using meteorological data for 15 June, 15 July, 15 August, and 15 September 2024. The corresponding peak solar irradiance values were 988.9, 945.3, 961.7, and 793.3 W/m^2. On 15 July, the absorber and outlet air temperatures reached 79.5℃ and 72.2℃, respectively; by 15 September, they had fallen to 70.9℃ and 63.7℃. The exergy calculations indicated that increasing the air mass flow rate from 0.002 to 0.023 kg/s reduced external exergy losses from 183 W to 17 W. Over the same flow-rate range, exergy destruction due to absorber-to-air heat transfer declined from a maximum of 11.5 W to 1 W, whereas friction-related exergy destruction rose from 1 W to 4.9 W. These results highlight the importance of evaluating both energy performance and exergy-related losses and irreversibility when assessing SAH operation.

Keywords: Solar air heater; mathematical model; energy balance; exergy balance; exergy destruction; heat transfer; air mass flow rate; solar irradiance; turbulator; thermodynamic efficiency.

Introduction

Solar energy is an important renewable resource for supplying heat at low and medium temperature levels. Among the available solar thermal technologies, solar air heaters are attractive because of their relatively simple design, low operating costs, and suitability for different thermal applications[1,2]. These characteristics make solar air heaters (SAHs) relevant to building heating and agricultural product drying[3]. However, their practical performance is influenced by several interacting factors, including changes in solar irradiance, ambient air temperature, airflow rate, thermal losses, and heat exchange between the absorber and the flowing air[4]. Although ribs and artificial surface roughness can enhance heat transfer, they may also increase pressure drop and fan power consumption. Consequently, an improvement in thermal efficiency does not always result in better overall thermodynamic performance[5]. The first law of thermodynamics provides a basis for quantifying energy input and useful heat output, but it does not fully account for the loss of energy quality associated with heat transfer, friction, pressure drop, and other irreversible processes. For this reason, a mathematical framework combining energy and exergy balances is required to assess SAH performance under changing climatic and operating conditions. Such an approach enables the evaluation of useful heat gain, energy losses, thermodynamic irreversibilities, and operating parameters that influence system performance[6]. Despite progress in SAH research, the comprehensive evaluation of energy and exergy performance under simultaneously varying solar irradiance, ambient temperature, and airflow conditions remains insufficiently addressed within a unified mathematical framework. Therefore, this study aims to develop a mathematical model of the energy and exergy balances of an SAH under variable climatic and operating conditions and to determine how the principal operating parameters affect its performance.

Literature Review: Research on SAHs has largely addressed methods for improving heat transfer, limiting airflow resistance, and enhancing energy and exergy performance. Tuncer et al. assessed parallel-flow, double-pass, and V-groove triple-pass SAH configurations through experiments and computational fluid dynamics (CFD) simulations. Their findings indicated that thermal efficiency could reach 90.65% and exergy efficiency 18.95%, with the difference between simulated and measured results not exceeding 10%[7]. Farhan et al. developed mathematical and numerical models for a V-corrugated SAH incorporating twisted-tape inserts. Their analysis showed that the Reynolds number, channel count, and twisted-tape ratio substantially influenced energy and thermohydraulic performance[8].

Abo-Elfadl et al. examined a tubular SAH incorporating porous material and reported an 8.9% improvement in energy efficiency and an 8.2% increase in exergy efficiency. Collectively, these studies demonstrate the potential of design

modifications to improve SAH performance while emphasizing the need to account for their effects on flow resistance and operating conditions[9].

Exergy analysis provides an additional means of assessing SAHs by examining energy quality, thermodynamic irreversibilities, and associated losses. Nidhul et al. integrated computational fluid dynamics (CFD) simulations with experimental testing of an SAH incorporating modified baffles, obtaining collector efficiencies of 55-70% and exergy efficiencies of 1.5-2.2%[10]. Khanlari et al. examined a vertical SAH fitted with a perforated baffle and a nano-modified absorber surface. The maximum difference between measured and simulated outlet air temperatures was 4.74%, while the nano-coating yielded exergy efficiencies of 9.25-10.58%[11]. Ghritlahre et al., in a review covering different SAH designs, highlighted the value of using both the first and second laws of thermodynamics to evaluate system performance[2]. Avargani et al. assessed the energy, exergy, enviro-exergy, and thermohydraulic characteristics of a flat-plate SAH with different baffle arrangements. Their findings showed that selected configurations increased energy efficiency by up to 39.2% and exergy performance by up to 103.2%[5]. These results indicate that SAH assessment should consider not only useful heat production but also exergy losses and irreversible processes.

Recent investigations of SAHs have increasingly combined theoretical modelling, computational simulations, and experimental validation. Tuncer et al. assessed the reliability of a CFD model by comparing its predictions with measured data, while Farhan et al. developed analytical and numerical approaches incorporating real-time meteorological information[7,8]. A systematic review published in 2023 examined SAHs from energy, exergy, exergoeconomic, and exergo environmental perspectives. It identified fluctuating solar irradiance and inadequate energy-storage capacity as important obstacles to uninterrupted system operation[12]. Under hot climatic conditions, Hassan et al. tested a tubular SAH with a nabla-shaped configuration and obtained average daily energy and exergy efficiencies of 88.4% and 3.89%, respectively[13]. Hegde et al. evaluated a cross-flow collector featuring a perforated absorber at Reynolds numbers between 3000 and 21000, achieving a peak exergy efficiency of 5.28%[14]. In another experimental investigation, Borah et al. found that square baffles combined with pin-type ribs on the absorber could raise energy and exergy efficiencies by as much as 32% while lowering exergy destruction by 10%.

Research from 2024-2025 has increasingly examined the combined influence of design features and operating conditions on SAH performance[15]. Abd et al. tested a double-pass collector incorporating a V-corrugated wire-mesh absorber and recorded peak energy and exergy efficiencies of 87.3% and 4.4%, respectively, at airflow rates of 0.01-0.03 kg/s[16]. Using numerical simulations, Arun Kumar et al. assessed the geometric characteristics of a multi-inlet SAH and obtained a thermohydraulic efficiency of 84.5% when the channel-width ratio was 3.3[17]. Vyas et al. examined airfoil-shaped and bio-inspired ribs in a double-pass design, analysing heat-transfer enhancement alongside hydraulic resistance for Reynolds numbers of 3000-21000. Their work also established mathematical correlations for predicting the Nusselt number and friction factor[18]. Hegde et al. investigated how changes to the side-wall geometry affected SAH thermohydraulic and exergy performance over a Reynolds number range of 3000-24000. The best-performing configuration yielded efficiencies of 85.65% and 4.08%, respectively. Overall, these studies show that SAH performance is governed by the interaction of collector geometry with operating variables, particularly airflow rate, Reynolds number, and fluctuations in solar irradiance[19].

Research conducted in 2025-2026 reflects a growing interest in combining conventional CFD simulations and experimental testing with optimization methods and data-driven modelling. Zhang et al. examined an active SAH through numerical simulations and experiments, demonstrating that optimizing design characteristics together with operating parameters can improve exergy efficiency[20]. A study published in 2026 explored deep learning as a means of predicting the thermohydraulic and exergy performance of an SAH fitted with a bidirectional wavy absorber. The investigation assessed how Reynolds number, wave amplitude, and geometric dimensions influence system performance[21]. Despite these advances, much of the existing research remains focused on individual collector designs or selected operating conditions investigated in laboratory environments. Mathematical models that incorporate time-dependent changes in solar irradiance, ambient temperature, airflow rate, and thermal losses into unified energy and exergy balances are still limited. Moreover, further work is needed to integrate inlet and outlet air temperatures, useful heat gain, thermal and pressure losses, exergy destruction, and total exergy efficiency into a single framework applicable to real climatic conditions. Developing an energy-exergy model that accounts for changing environmental and operating parameters is therefore important for evaluating actual SAH performance, identifying dominant loss mechanisms, and establishing suitable operating conditions.

Materials and Methods

Study Location and Climatic Conditions: The investigation was carried out in Qarshi, Kashkadarya Region, Uzbekistan, at geographical coordinates of 38.75° N and 65.72° E. The local climate is dry and continental, characterized by intense solar radiation, limited rainfall, low relative humidity, and pronounced daily and seasonal temperature fluctuations. To examine SAH performance under different seasonal conditions, meteorological data collected on 15 June, 15 July, 15 August, and 15 September 2024 were used as input for the calculations. On each of these dates, solar irradiance and ambient air temperature were recorded continuously between 08:00 and 18:00, as illustrated in Figure-1.

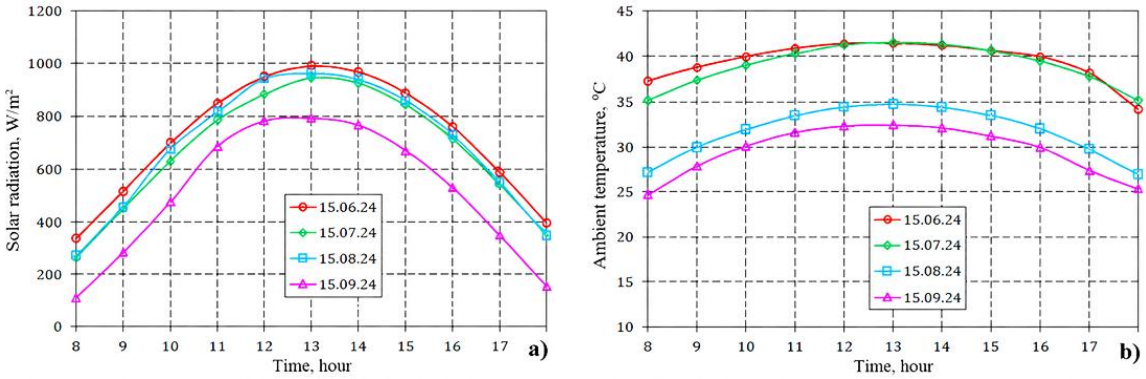


Figure-1: Daily profiles of (a) solar irradiance and (b) ambient air temperature measured in Qarshi on 15 June, 15 July, 15 August, and 15 September 2024.

Figure-1(a) illustrates how solar irradiance changed throughout the day on the four selected dates in 2024. In each case, irradiance rose during the morning, peaked at approximately 13:00, and then declined. The recorded peak values were 988.9 W/m^2 on 15 June, 945.3 W/m^2 on 15 July, 961.7 W/m^2 on 15 August, and 793.3 W/m^2 on 15 September. The September maximum was substantially below those measured from June through August, demonstrating the seasonal variation in solar energy available to the SAH. This variation is an important external factor influencing collector energy performance.

Figure-1(b) depicts the corresponding changes in ambient air temperature. On 15 June and 15 July, the temperature at 08:00 ranged from 34.2 to 35.2℃, rising to approximately 41-42℃ between 13:00 and 14:00. The peak temperature on 15 August was approximately 34.7℃, compared with around 32.4℃ on 15 September. After 13:00, ambient temperature gradually declined on all four dates. The measured solar irradiance and ambient temperature profiles were used as input data and boundary conditions for evaluating the SAH thermal balance, useful heat gain, and exergy efficiency.

SAH Configuration and Assumptions Adopted for the Mathematical Model: The mathematical investigation was based on a SAH with a length of 1.0 m, a width of 0.5 m, and a structural height of 0.06 m. These dimensions correspond to a total working area of 0.5 m^2. Internal baffles were incorporated to redirect the air stream through an extended flow path, promoting heat exchange between the absorber and the flowing air. The air inlet was positioned on one side of the collector, whereas the heated-air outlet was placed on the opposite side (Figure-2).

The baffle arrangement divided the internal passage into successive flow channels, increasing contact between the air and the heat-transfer surface. The collector geometry and internal arrangement served as key model parameters for describing heat transfer and airflow behaviour. The mathematical formulation was developed using the following assumptions: airflow inside the SAH is represented by a one-dimensional mean flow; air thermophysical properties vary with the mean temperature over the calculation interval; and, although heat conduction occurs within the collector structure, the dominant heat-transfer direction is from the absorber to the air stream. Solar irradiance is treated as a time-dependent input, while ambient air temperature defines a boundary condition for estimating heat losses from the collector. In addition to heat transfer to the flowing air, hydraulic pressure losses are included in the exergy analysis.

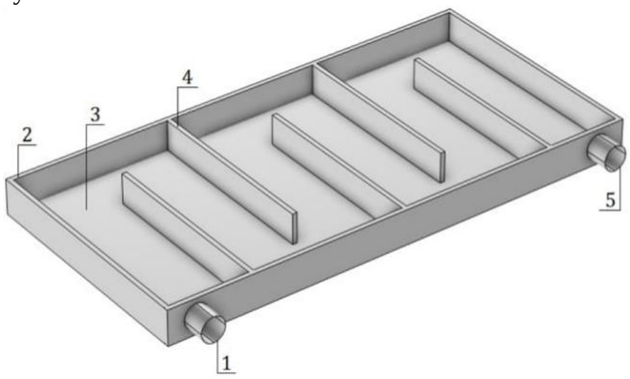


Figure-2: Schematic configuration of the SAH equipped with internal baffles: 1-air inlet; 2-SAH casing; 3-absorber surface; 4-internal baffle (turbulator); 5-air outlet.

Mathematical Model for the Energy Balance: Based on the assumptions outlined above, energy balance equations were established for each component of the SAH. The energy balance for the transparent glass cover is expressed as:

$$Q_{cov} = I_s + Q_{r,ab-cov} - Q_{c,cov-a} - Q_{c,cov-amb} - Q_{r,cov-sky} \quad (1)$$

The rate of energy accumulation in the transparent cover is determined by:

$$Q_{cov} = \rho_{cov} V_{cov} c_{p,cov} \frac{dt_{cov}}{d\tau} \quad (2)$$

Where ρ_{cov} is the density of the transparent cover (kg/m^3), V_{cov} denotes its volume (m^3), and $c_{p,cov}$ represents its specific heat capacity (J/(kg·℃)). The solar power absorbed by the cover, I_s, is calculated as:

$$I_s = \alpha_{cov} S_{cov} F_{cov} \quad (3)$$

Here, α_{cov} is the radiation absorption coefficient of the transparent cover, S_{cov} denotes the incident solar radiation flux density (W/m²), and F_{cov} is the surface area of the cover (m²).Radiative heat transfer between the absorber and the transparent cover is expressed as:

$$Q_{r,ab-cov} = h_{r,ab-cov}(t_{ab} - t_{cov})F_{cov} \quad (4)$$

The convective heat-transfer rate between the cover and the air is calculated using:

$$Q_{c,cov-a} = h_{c,cov-a}(t_{cov} - t_a)F_{cov} \quad (5)$$

Heat transfer by convection between the transparent cover and the ambient environment is described by:

$$Q_{c,cov-amb} = h_{c,cov-amb}(t_{cov} - t_{amb})F_{cov} \quad (6)$$

Radiative heat exchange between the transparent cover and the sky is determined from:

$$Q_{r,cov-sky} = h_{r,cov-sky}(t_{cov} - t_{sky})F_{cov} \quad (7)$$

For the absorber of the SAH equipped with turbulators, the energy balance is expressed as:

$$Q_{ab} = I_{ab} - Q_{r,ab-cov} - Q_{c,ab-a} - Q_{c,t-a} - Q_{cd,ab-amb} \quad (8)$$

The rate of energy accumulation in the absorber is calculated as:

$$Q_{ab} = \rho_{ab} V_{ab} c_{p,ab} \frac{dt_{ab}}{d\tau} \quad (9)$$

where ρ_{ab} denotes the absorber density (kg/m³), V_{ab} is its volume (m³), and $c_{p,ab}$ represents its specific heat capacity (J/(kg·°C)). The solar power absorbed by the absorber, I_{ab}, is determined by:

$$I_{ab} = \tau_{cov} \alpha_{ab} S_{ab} F_{ab} \quad (10)$$

Here, τ_{cov} is the transmittance of the transparent cover, α_{ab} represents the absorber's solar-radiation absorption coefficient, S_{ab} denotes the incident solar irradiance (W/m²), and F_{ab} is the absorber surface area (m²). The radiative heat-transfer rate between the absorber and the transparent cover, $Q_{r,ab-cov}$, is calculated using Equation (4). Convective heat transfer from the absorber to the air is expressed as:

$$Q_{c,ab-a} = h_{c,ab-a}(t_{ab} - t_a)F_{ab} \quad (11)$$

The convective heat-transfer rate between the turbulators and the airflow is given by:

$$Q_{c,t-a} = h_{c,t-a}(t_t - t_a)F_t \quad (12)$$

Heat transfer between the absorber and the ambient environment is represented by:

$$Q_{cd,ab-amb} = h_{cd,ab-amb}(t_{ab} - t_{amb})F_{ab} \quad (13)$$

For the air flowing through the SAH, the heat gained from the cover and absorber is expressed as:

$$Q_a = Q_{c,cov-a} + Q_{c,ab-a} \quad (14)$$

The quantity Q_a represents the useful energy gained by the air inside the SAH.

$$Q_a = \rho_a V_a c_{p,a} \frac{dt_a}{d\tau} \quad (15)$$

The air properties used in the model are defined as follows: ρ_a denotes air density (kg/m³), V_a is the air volume (m³), and $c_{p,a}$ represents the specific heat capacity of air (J/(kg·°C)). The convective heat-transfer rate between the absorber and the airflow, $Q_{c,ab-a}$, is calculated using Equation (11).

The heat-transfer coefficients appearing in Equation (1)-(15) are evaluated using the following relationships. The coefficient describing convective heat exchange between the transparent cover and the surrounding air, including the effect of wind, is calculated according to C. D. Ho et al.[22]:

$$h_{c,cov-amb} = 2{,}8 + 3w_w \quad (16)$$

wherew_w denotes wind velocity (m/s).

The radiative heat-transfer coefficient between the transparent cover and the sky is determined using Verma R. et al.[23]:

$$h_{r,cov-sky} = \sigma \varepsilon_{cov}(t_{cov} + t_{sky})(t_{cov}^2 + t_{sky}^2)\frac{(t_{cov} - t_{sky})}{(t_{cov} - t_{amb})} \quad (17)$$

Here, σ is the Stefan-Boltzmann constant, ε_{cov} denotes the emissivity of the transparent cover, t_{cov} is its temperature (°C), and t_{sky} represents the effective sky temperature (°C). The latter is estimated from the ambient air temperature using:

$$t_{sky} = t_{amb} - 6 \quad (18)$$

Where t_{amb} is the ambient air temperature (°C).

The radiative heat-transfer coefficient between the absorber and the transparent cover is calculated according to Lin, W. et al.[24]

$$h_{r,ab-cov} = \frac{\sigma(t_{ab}^2 + t_{cov}^2)(t_{ab} + t_{cov})}{\frac{1}{\varepsilon_{ab}} + \frac{1}{\varepsilon_{cov}} - 1} \quad (19)$$

wheret_{ab} is the absorber temperature (°C), and ε_{ab} denotes its emissivity.

The convective heat-transfer coefficient between the airflow and the transparent cover is expressed as:

$$h_{c,cov-a} = Nu_1 \frac{k}{d_h} \quad (20)$$

The hydraulic diameter of the SAH air passage, d_h, is calculated from the channel dimensions as follows:

$$d_h = \frac{2WH}{W+H} \quad (21)$$

where W denotes the channel width (m), and H represents its height (m).

The Nusselt number Nu_1 is evaluated using the correlations reported in Fudholi A. et al.[25] with the appropriate expression selected according to the Reynolds number.

For $Re < 2300$

$$Nu_1 = 5{,}4 + \frac{0{,}00190\left[Re_1 Pr\left(\frac{d_h}{L}\right)^{1{,}71}\right]}{1+0{,}00563\left[Re_1 Pr\left(\frac{d_h}{L}\right)^{1{,}17}\right]} \quad (22)$$

For $2300 < Re < 6000$

$$Nu_1 = 0{,}116\left(Re_1^{2/3} - 125\right)Pr^{1/3} + \left[1 + \left[\frac{d_h}{L}\right]^{2/3}\right]\left[\frac{\mu}{\mu_w}\right]^{0{,}14} \quad (23)$$

For $Re > 6000$

$$Nu_1 = 0{,}018 Re_1^{0{,}8} Pr^{0{,}4} \quad (24)$$

Here, L is the length of the air channel (m), while μ and μ_w represent the dynamic viscosities of air and the channel wall, respectively (Pa·s).

The convective heat-transfer coefficient between the absorber and the airflow is determined using the following relationship:

$$h_{c,ab-a} = Nu_2 \frac{k}{d_h} \quad (25)$$

Where Nu_2 is the Nusselt number calculated using the correlation given in Saini S.K. and Saini R.P.[26]:

$$Nu_2 = 0{,}001047 Re_2^{1{,}3186} \left(\frac{e}{d_h}\right)^{0{,}3772} \left(\frac{\alpha}{90}\right)^{-0{,}1198} \quad (26)$$

The ratio e/d_h represents the turbulator height relative to the hydraulic diameter of the SAH air channel.

The convective heat-transfer coefficient associated with heat exchange between the turbulator and the airflow is calculated as:

$$h_{c,t-a} = \frac{m c_{p,a}(t_a^{''} - t_a^{'})}{F_t(t_t - t_a)} \quad (27)$$

where m denotes the air mass flow rate (kg/s), $c_{p,a}$ is the specific heat capacity of air, $t_a^{'}$ and $t_a^{''}$ are the inlet and outlet air temperatures (°C), respectively, F_t is the turbulator surface area (m^2), and t_t and t_a represent the turbulator and air temperatures (°C).

The coefficient used to characterize conductive heat transfer from the absorber toward the ambient environment is expressed as:

$$h_{cd,ab-amb} = \frac{k_{in}}{\delta_{in}} \quad (28)$$

Here, k_{in} denotes the thermal conductivity of the insulating material, while δ_{in} represents its thickness.

Using the previously established energy-balance equations and the corresponding heat-transfer relationships, expressions can be derived to calculate the temperatures of the transparent cover, absorber, and heated air.

For the transparent cover, the governing differential equation is obtained by combining the energy accumulation term with the absorbed solar energy and the radiative and convective heat-transfer terms:

$$\rho_{cov} V_{cov} c_{p,cov} \frac{dt_{cov}}{d\tau} = \alpha_{cov} S_{cov} F_{cov} + h_{r,ab-cov}(t_{ab} - t_{cov}) F_{ab} - h_{c,cov-a}(t_{cov} - t_a) F_{cov} - -h_{c.cov-amb}(t_{cov} - t_{amb}) F_{cov} - h_{r,cov-sky}(t_{cov} - t_{sky}) F_{cov} \quad (29)$$

For the absorber, the energy balance is written as:

$$\rho_{ab} V_{ab} c_{p,ab} \frac{dt_{ab}}{d\tau} = \tau_{cov} \alpha_{ab} S_{ab} F_{ab} - h_{r,ab-cov}(t_{ab} - t_{cov}) F_{ab} - -h_{c,ab-a}(t_{ab} - t_a) F_{ab} - h_{c,t-a}(t_t - t_a) F_t - h_{cd,ab-amb}(t_{ab} - tambFab \quad (30)$$

For the heated air, the corresponding equation is:

$$\rho_a V_a c_{p,a} \frac{dt_a}{d\tau} = h_{c,cov-a}(t_{cov} - t_a) F_{cov} + h_{c,ab-a}(t_{ab} - t_a) F_{ab} \quad (31)$$

The input parameters used in the numerical analysis of the turbulator-equipped SAH are summarized in Table-1.

Table-1: Thermophysical and geometric parameters used in the mathematical model.

Parameter	Value	Parameter	Value
F_{cov}	0,5 m^2	h_{ab-amb}	5 $W/(m^2 \cdot ℃)$
F_{ab}	0,5 m^2	α_{cov}	0,06
F_{in}	0,66 m^2	α_{ab}	0,95
$c_{p,cov}$	840 $J/(kg \cdot ℃)$	ε_{cov}	0,9
$c_{p,ab}$	860 $J/(kg \cdot ℃)$	ε_{ab}	0,94
V_{cov}	0,002 m^3	τ_{cov}	0,84
m_{ab}	4,1 kg	w_a	2 m/s
ρ_{cov}	2700 kg/m^3	ν_a	$1{,}88 \cdot 10^{-5} m^2/s$
w_w	2…5 m/s	F_t	0,096 m^2
P	3 m	k_{in}	0,034 $W/(m \cdot ℃)$
W	0,5 m	δ_{in}	0,02 m
H	0,06 m	δ_{ab}	0,002 m
ρ_{ab}	2530 kg/m^3	V_{ab}	0,0015 m^3

The energy-balance model was used to quantify the conversion of solar radiation into useful heat and to estimate thermal losses from the SAH.

However, evaluating energy quality and the irreversible processes occurring within the system also requires an exergy assessment. Accordingly, the following section develops the exergy model for the SAH.

Mathematical Model for the Exergy Balance: Whereas the energy balance quantifies the energy supplied to and released from the SAH, exergy analysis evaluates the work potential of that energy and identifies thermodynamic irreversibilities.

The analysis accounts for exergy transfer associated with solar irradiation, airflow through the collector, and interactions with the surrounding environment. Based on this approach, equations are formulated to determine exergy input, useful exergy output, exergy destruction, and the overall exergy efficiency. The assumptions underlying this analysis are detailed in Bayrak F.[27], Kurtbaş İ. and Durmuş A.[28]. Treating the SAH as a control volume, its exergy balance is written as follows, according to Velmurugan P. and Kalaivanan R.[29]:

$$\sum Ex_{en,net} - \sum Ex_{lea,net} = \sum Ex_{des} \quad (32)$$

Here, the subscript *net* denotes the net exergy contribution. The terms $\sum Ex_{en,net}$ and $\sum Ex_{lea,net}$ represent the total exergy entering and leaving the control volume, respectively, whereas $\sum Ex_{des}$ denotes the exergy destroyed within the system.

The net exergy supplied to the SAH is associated with incoming solar radiation and is calculated using Sabzpooshani M.[30]:

$$\sum Ex_{en,net} = Ex_{sol} = I F_{SAH} \left[1 - \frac{4}{3}\left(\frac{t_{amb}}{t_{sol}}\right) + \frac{1}{3}\left(\frac{t_{amb}}{t_{sol}}\right)^4\right] \quad (33)$$

Where t_{sol} is the solar temperature.

The total exergy destruction rate includes both exergy losses across the control-volume boundary and irreversibilities generated inside the system, as described in Kotas T. J.[31]:

$$\sum Ex_{d} = \sum Ex_{d.out} + \sum Ex_{d.in} \quad (34)$$

The exergy that crosses the control-volume boundary and is no longer available for use is classified as external exergy loss. This category includes losses associated with friction, fluid mixing, and exergy transfers that do not remain within the control volume. In contrast, internal exergy destruction refers to the loss of useful work potential caused by irreversible processes occurring inside the system. Accordingly, Equation (34) can be expressed in terms of the individual exergy-loss contributions as follows:

$$\sum Ex_{des} = Ex_{opt} + Ex_{Q} + Ex_{ab-s} + Ex_{ab-a} + Ex_{fric} \quad (35)$$

Each of these components is considered separately. Ex_{opt} represents the optical exergy loss from the SAH surface.

$$Ex_{opt} = I F_{cov} (1 - \alpha_{ab} \tau_{cov}) \left[1 - \frac{4}{3}\left(\frac{t_{amb}}{t_{sol}}\right) + \frac{1}{3}\left(\frac{t_{amb}}{t_{sol}}\right)^4\right] \quad (36)$$

The exergy loss associated with heat escaping from the SAH to the surrounding environment is calculated as follows:

$$Ex_{Q} = U F_{ab} (t_{ab} - t_{amb}) \left[1 - \left(\frac{t_{amb}}{t_{ab}}\right)\right] \quad (37)$$

Here, $U = U_{ov} + U_{up}$, where U_{ov} denotes the overall heat-loss coefficient, determined using Equation (28), and U_{up} represents the heat-loss coefficient for the upper part of the collector. The latter is calculated from:

$$U_{up} = \left[\frac{1}{h_{r,ab-cov} + h_{c,cov-a}} + \frac{1}{h_{r,cov-sol} + h_{c,cov-amb}}\right]^{-1} \quad (38)$$

The rate of exergy destruction associated with solar radiation absorbed by the absorber plate is expressed as:

$$Ex_{ab-sol} = I F_{ab} \alpha_{ab} \tau_{cov} \left[1 - \frac{4}{3}\left(\frac{t_{amb}}{t_{sol}}\right) + \frac{1}{3}\left(\frac{t_{amb}}{t_{sol}}\right)^4 - 1 - \square\square\square\square\square\square\square\square\right] \quad (39)$$

Exergy destruction resulting from heat transfer between the absorber surface and the working fluid is calculated using:

$$Ex_{ab-a} = I F_{ab} \eta t_{amb} \left[\frac{1}{t_a} - \frac{1}{t_{ab}}\right] \quad (40)$$

where the mean air temperature is defined as: $t_a = (t'_a + t''_a)/2$.

The exergy loss associated with friction as air passes through the SAH channel is determined from:

$$Ex_{fric} = \frac{t_{amb} m_a \Delta P}{\rho_a t_a} \quad (41)$$

The input parameters used to determine the exergy efficiency of the turbulator-equipped SAH are listed in Table-2.

Using the developed energy and exergy models, numerical calculations are performed to assess heat transfer, useful thermal

output, and thermodynamic losses under varying climatic and operating conditions.

Solar irradiance, ambient air temperature, air mass flow rate, and the collector's geometric and thermophysical characteristics are incorporated as the principal input variables and boundary conditions.

The subsequent Results and Discussion section presents and interprets the calculated results, examining the energy and exergy efficiencies of the SAH and the influence of key operating parameters on these performance indicators.

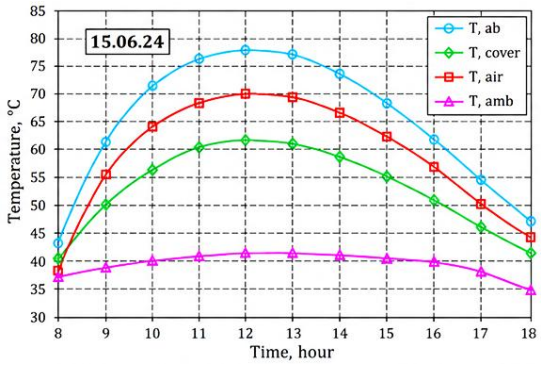
Table-2: Geometric and operating parameters of the SAH.

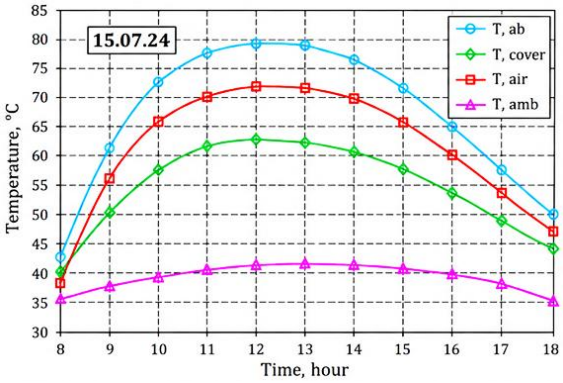
Parameter	Value
Length, m	1
Width, m	0,5
Depth, m	0,06
Insulation material thickness, m	0,02
Thermal conductivity of insulation, $W/(m\cdot℃)$	0,034
Absorber emissivity	0,9
Transparent cover emissivity	0,88
Product of transmittance and absorptance coefficients	0,8
Ambient temperature, ℃	27
Wind speed, m/s	1,5
Turbulator-to-hydraulic-diameter ratio	0,042
Airflow inlet angle	90
Solar temperature,℃	5500
Air mass flow rate, kg/s	0,002..0,023
Solarradiation, W/m^2	700...1000

Results and Discussion

Temperature Distribution of the SAH Based on the Energy Balance: The energy-balance model was used to determine the thermal behaviour of the solar air heater (SAH) equipped with turbulators, and the calculated temperature profiles are presented in Figure-3. The figure illustrates the changes in absorber-surface, transparent-cover, outlet-air, and ambient-air temperatures on 15 June, 15 July, 15 August, and 15 September 2024. For all four dates, the temperature profiles followed the daily solar-radiation pattern: temperatures rose during the morning, approached their highest levels around midday, and declined thereafter. This correspondence indicates that the thermal response of the SAH is strongly influenced by changes in solar irradiance and ambient temperature. On 15 June 2024, the absorber temperature increased to approximately 77.9℃, while the transparent cover and outlet air temperatures reached maximum values of 61.6℃ and 70.0℃, respectively.

The ambient air temperature reached approximately 41.4℃ during this period. On 15 July 2024, the maximum absorber and outlet air temperatures were approximately 79.5℃ and 72.2℃, respectively, representing the highest values observed during the investigated period. The transparent cover temperature increased to approximately 62.9℃, while the ambient air temperature was around 42.3℃.





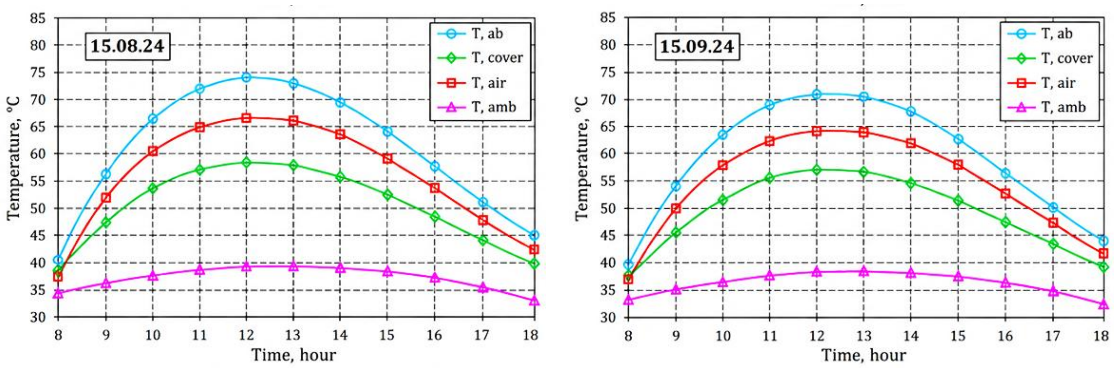


Figure-3: Daily temperature profiles of the absorber, transparent cover, outlet air, and ambient air on 15 June, 15 July, 15 August, and 15 September 2024.

On 15 August 2024, the absorber reached a maximum temperature of approximately 73.4℃, while the outlet air and transparent cover reached 66.0℃ and 58.1℃, respectively. By 15 September, the corresponding values had fallen to 70.9℃, 63.7℃, and approximately 56.1℃. This decline is consistent with the lower solar irradiance recorded in September. Across all selected dates, the absorber exhibited the highest temperature, whereas the ambient air remained the coolest component. The temperature difference between the absorber and the outlet air reflects heat transfer from the absorber to the flowing air. Meanwhile, the lower temperature of the transparent cover indicates heat exchange between the collector and its surroundings, including heat losses through the upper surface.

The highest temperatures generally occurred between 12:00 and 13:00, followed by a gradual decline. This pattern corresponds to the daily solar-radiation profiles shown in Figure-1, confirming the close relationship between solar input and the thermal response of the SAH. Overall, the collector operated at higher temperatures in June and July, whereas August and particularly September exhibited cooler conditions because of reduced solar irradiance. These temperature profiles provide a basis for subsequent calculations of useful heat output and the energy and exergy efficiencies of the SAH.

Analysis of Exergy Losses and Exergy Destruction in the SAH: Using the operating parameters listed in Table-2, Figure-4 illustrates how changes in air mass flow rate affect exergy losses and exergy destruction in the SAH.

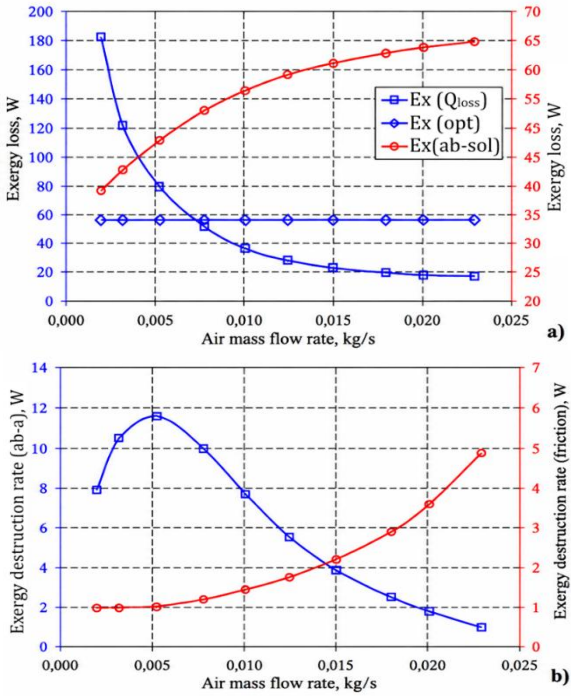


Figure-4: Dependence of exergy losses and exergy destruction rates on air mass flow rate in the SAH.

Figure-4 illustrates how the air mass flow rate influences exergy losses and exergy destruction in the SAH. The results indicate that varying the mass flow rate between 0.002 and 0.023 kg/s affects both the magnitude and distribution of exergy losses throughout the system. As shown in Figure-4(a), the exergy loss associated with heat transfer to the surroundings, $Ex(Q_{loss})$, decreases markedly as the airflow rate increases. Its value falls from approximately 183 W at 0.002 kg/s to 80 W at 0.005 kg/s, 37 W at 0.010 kg/s, and 17 W at 0.023 kg/s.

This trend suggests that higher airflow rates alter the collector's heat-transfer conditions and reduce exergy losses to the environment. By comparison, the optical exergy loss, Ex(opt), remains nearly unchanged at approximately 56 W across the investigated range, indicating little sensitivity to airflow rate.

The exergy destruction associated with solar radiation absorption, Ex(ab-a), follows the opposite trend, increasing from around 39 W at 0.002 kg/s to 56 W at 0.010 kg/s, 61 W at 0.015 kg/s, and approximately 65 W at 0.023 kg/s. Thus, increasing airflow reduces certain exergy losses while increasing the contribution associated with solar energy absorption.

Figure-4(b) describes the dependence of exergy destruction due to absorber-to-air heat transfer and airflow friction on the mass flow rate. Heat-transfer-related exergy destruction initially rises, reaching approximately 11.5 W at a flow rate of 0.005 kg/s. At higher flow rates, this component decreases, whereas friction-related exergy destruction increases as the airflow rate rises.

As the air mass flow rate increases further, exergy destruction associated with absorber-to-air heat transfer declines steadily, reaching approximately 4 W at 0.015 kg/s, 2 W at 0.020 kg/s, and about 1 W at 0.023 kg/s. This behaviour can be attributed to the decreasing temperature difference between the absorber and the airflow, which reduces thermodynamic irreversibility during heat exchange.

In contrast, exergy destruction caused by airflow friction rises continuously with increasing mass flow rate. It increases from approximately 1 W at 0.002 kg/s to 1.4 W at 0.010 kg/s, 2.2 W at 0.015 kg/s, 3.5 W at 0.020 kg/s, and 4.9 W at 0.023 kg/s. This increase reflects the greater pressure losses associated with higher air velocity and hydraulic resistance.

Overall, Figure-4 demonstrates that airflow rate influences SAH exergy performance through two competing effects: higher flow rates reduce heat-transfer-related exergy destruction and external thermal losses, but increase friction-related exergy destruction.

Consequently, evaluating SAH exergy efficiency requires balancing improvements in heat transfer against the additional thermodynamic losses caused by airflow resistance.

Conclusion

The developed mathematical framework was applied to assess the thermal response and thermodynamic performance of a turbulator-equipped SAH under changing environmental and operating conditions. For Qarshi, the peak solar irradiance recorded on 15 June, 15 July, 15 August, and 15 September was 988.9, 945.3, 961.7, and 793.3 W/m^2, respectively, confirming a reduction in available solar input by September. The energy-balance results showed that, on 15 July, the absorber, outlet air, and transparent cover reached maximum temperatures of 79.5℃, 72.2℃, and 62.9℃, respectively. By 15 September, these temperatures had declined to 70.9℃, 63.7℃, and 56.1℃.

The exergy assessment revealed a strong dependence on air mass flow rate. When the flow rate increased from 0.002 to 0.023 kg/s, exergy loss to the surroundings fell from 183 W to 17 W, whereas optical exergy loss remained approximately 56 W. Exergy destruction associated with heat transfer between the absorber and air peaked at 11.5 W at 0.005 kg/s and then decreased to about 1 W at 0.023 kg/s. Conversely, friction-related exergy destruction increased from 1 W to 4.9 W over the same flow-rate range. These findings demonstrate that higher airflow can limit external thermal losses and heat-transfer-related irreversibilities, but it also intensifies hydraulic resistance and friction losses. Therefore, selecting suitable SAH operating conditions requires a balanced assessment of heat-transfer performance and airflow-related exergy destruction.

Overall, the proposed mathematical model provides an integrated means of assessing the thermal and thermodynamic behaviour of a turbulator-equipped SAH under changing climatic and operating conditions. The findings indicate that fluctuations in solar irradiance, ambient temperature, and air mass flow rate influence the collector's temperature distribution, exergy losses, and internal irreversibilities. Evaluating heat-transfer enhancement alongside hydraulic resistance therefore enables a more complete characterization of SAH performance and helps identify suitable operating regimes. This combined energy-exergy framework can support the further optimization and reliable operation of SAH systems under real climatic conditions.

References

1. Kabeel, A.E., Hamed, M.H., Omara, Z.M., &Kandeal, A.W. (2017). Solar air heaters: Design configurations, improvement methods and applications - A detailed review. *Renewable and Sustainable Energy Reviews*, 70, 1189-1206.

2. Ghritlahre, H.K., Verma, M., Parihar, J.S., Mondloe, D.S., & Agrawal, S. (2022). A detailed review of various types of solar air heaters performance. *Solar Energy*, 237, 173-195.

3. Öztop, H.F., Bayrak, F., &Hepbasli, A. (2013). Energetic and exergetic aspects of solar air heating (solar collector) systems. *Renewable and Sustainable Energy Reviews*, 21, 59-83.

4. Hassan, A., Nikbakht, A.M., Fawzia, S., Yarlagadda, P., & Karim, A. (2024). A comprehensive review of the thermohydraulic improvement potentials in solar air heaters through an energy and exergy analysis. *Energies*, 17(7), 1526.

5. Avargani, V.M., Zendehboudi, S., Rahimi, A., &Soltani, S. (2022). Comprehensive energy, exergy, enviro-exergy, and thermo-hydraulic performance assessment of a flat plate solar air heater with different obstacles. *Applied Thermal Engineering*, 203, 117907.

6. Tchinda, R. (2009). A review of the mathematical models for predicting solar air heaters systems. *Renewable and Sustainable Energy Reviews*, 13(8), 1734-1759.

7. Tuncer, A.D., Khanlari, A., Sözen, A., Gürbüz, E.Y., Şirin, C., & Gungor, A. (2020). Energy-exergy and enviro-economic survey of solar air heaters with various air channel modifications. *Renewable Energy*, 160, 67-85.

8. Farhan, A.A., Aljubury, I.M.A., & Ahmed, H.E. (2021). Energetic and exergetic efficiency analysis of a V-corrugated solar air heater integrated with twisted tape inserts. *Renewable Energy*, 169, 1373-1385.

9. Abo-Elfadl, S., Yousef, M.S., El-Dosoky, M.F., & Hassan, H. (2021). Energy, exergy, and economic analysis of tubular solar air heater with porous material: An experimental study. *Applied Thermal Engineering*, 196, 117294.

10. Nidhul, K., Yadav, A.K., Anish, S., &Arunachala, U.C. (2022). Thermo-hydraulic and exergetic performance of a cost-effective solar air heater: CFD and experimental study. *Renewable Energy*, 184, 627-641.

11. Khanlari, A., Tuncer, A.D., Sözen, A., Aytaç, İ., Çiftçi, E., & Variyenli, H.İ. (2022). Energy and exergy analysis of a vertical solar air heater with nano-enhanced absorber coating and perforated baffles. *Renewable Energy*, 187, 586-602.

12. Pathak, S.K., Tyagi, V.V., Chopra, K., Kalidasan, B., Pandey, A.K., Goel, V., Saxena, A., & Ma, Z. (2023). Energy, exergy, economic and environmental analyses of solar air heating systems with and without thermal energy storage for sustainable development: A systematic review. *Journal of Energy Storage*, 59, 106521..

13. Hassan, H., Osman, O.O., Abdelmoez, M.N., & Abo-Elfadl, S. (2023). Energy and exergy evaluation of new design nabla shaped tubular solar air heater (∇TSAH): Experimental investigation. *Energy*, 276, 127451.

14. Hegde, A.K., Pai, R., & Karanth, K.V. (2023). Energy and exergy analysis of a cross flow solar air heater for thermohydraulic performance augmentation. *International Journal of Thermal Sciences*, 194, 108577.

15. Borah, P.P., Pathak, K.K., Gupta, A., Roy, S., & Das, B. (2023). Experimental study of a solar air heater with modified absorber plate through square obstacles with threaded pin fins. *Applied Thermal Engineering*, 228, 120544.

16. Abd, H.M., Abdulrazzaq, N.M., &Soheel, A.H. (2024). Solar air heater energy and exergy enhancement using a V-corrugated wire mesh absorber: An experimental comparison. *Energy*, 309.

17. Arunkumar, H. S., Kumar, S., & Karanth, K.V. (2024). Energy, exergy and economic analysis of a multiple inlet solar air heater for augmented thermohydraulic performance. *Applied Thermal Engineering*, 246, 122981.

18. Vyas, S., Sharma, A.K., & Rai, A.K. (2024). Double pass solar air heater with aerofoil and bio-inspired fins: A numerical analysis of thermohydraulic performance. *Energy*, 311, 133320.

19. Hegde, A.K., Pai, R. & Karanth, K.V. (2025). Energy and exergetic analysis of a solar air heater for enhanced thermohydraulic performance with side wall treatment. *Energy*, 315, 134333.

20. Zhang, Z., Beikpour, S., Ali, A.B.M., Jasim, D.J., Hasson, A.R., Abdullaev, S., Salahshour, S., &Hekmatifar, M. (2025). Experimental and numerical investigations of an active solar air heater: Energy and exergy analysis and optimization to increase the efficiency. *International Communications in Heat and Mass Transfer*, 169, 109744.

21. Li, D., Bai, Z., Samad, S., Abed, A.M., Li, Y., Alhumaid, S., Dutta, A.K., Alkhalaf, S., Nadeem Khan, M., &Elhosiny Ali, H. (2026). Deep learning-based prediction of thermal-hydraulic and exergy performance in a novel bidirectional wavy absorber solar air heater. *Renewable Energy*, 256, 124192.

22. Ho, C.D., Yeh, H. M. and Wang, R.C. (2005). Heat-transfer enhancement in double-pass flat-plate solar air heaters with recycle. *Energy*, 30(15), 2796-2817.

23. Verma, R., Chandra, R. & Garg, H.P. (1991). Parametric studies on the corrugated solar air heaters with and without cover. *Renewable Energy*, 1(3), 361-371.

24. Lin, W., Gao, W., & Liu, T. (2006). A parametric study on the thermal performance of cross-corrugated solar air collectors. *Applied Thermal Engineering*, 26(10), 1043-1053.

25. Fudholi, A., Sopian, K., Ruslan, M.H., & Othman, M.Y. (2013). Performance and cost benefits analysis of double-pass solar collector with and without fins. *Energy Conversion and Management*, 76, 8-19.

26. Saini, S.K., & Saini, R.P. (2008). Development of correlations for Nusselt number and friction factor for solar air heater with roughened duct having arc-shaped wire as artificial roughness. *Solar Energy*, 82(12), 1118-1130.

27. Bayrak, F., Öztop, H.F., & Hepbasli, A. (2013). Energy and exergy analyses of porous baffles inserted solar air heaters for building applications. *Energy and Buildings*, 57, 338-345.

28. Kurtbaş İ. and Durmuş A. (2004). Efficiency and exergy analysis of a new solar air heater. *Renewable Energy*, 29(9), 1489–1501.

29. Velmurugan P. and Kalaivanan R. (2015). Energy and exergy analysis of solar air heaters with varied geometries. *Arabian Journal for Science and Engineering*, 40(4), 1173-1186.

30. Sabzpooshani M., Mohammadi K. and Khorasanizadeh H. (2014). Exergetic performance evaluation of a single pass baffled solar air heater. *Energy*, 64, 697-706.

31. Kotas T. J. (2012). *The exergy method of thermal plant analysis*. Paragon Publishing.